GLOBAL CHANGE

Reprint 2017-22

Reprinted with permission from *Geoscientific Model Development*, 10: 2833–2848.
© 2017 the authors

The **MIT Joint Program on the Science and Policy of Global Change** combines cutting-edge scientific research with independent policy analysis to provide a solid foundation for the public and private decisions needed to mitigate and adapt to unavoidable global environmental changes. Being data-driven, the Joint Program uses extensive Earth system and economic data and models to produce quantitative analysis and predictions of the risks of climate change and the challenges of limiting human influence on the environment—essential knowledge for the international dialogue toward a global response to climate change.

To this end, the Joint Program brings together an interdisciplinary group from two established MIT research centers: the **Center for Global Change Science (CGCS)** and the **Center for Energy and Environmental Policy Research (CEEPR)**. These two centers—along with collaborators from the Marine Biology Laboratory (MBL) at Woods Hole and short- and long-term visitors—provide the united vision needed to solve global challenges.

At the heart of much of the program's work lies MIT's Integrated Global System Model. Through this integrated model, the program seeks to discover new interactions among natural and human climate system components; objectively assess uncertainty in economic and climate projections; critically and quantitatively analyze environmental management and policy proposals; understand complex connections among the many forces that will shape our future; and improve methods to model, monitor and verify greenhouse gas emissions and climatic impacts.

This reprint is intended to communicate research results and improve public understanding of global environment and energy challenges, thereby contributing to informed debate about climate change and the economic and social implications of policy alternatives.

—Ronald G. Prinn and John M. Reilly,
Joint Program Co-Directors

MIT Joint Program on the Science and Policy of Global Change

Massachusetts Institute of Technology
77 Massachusetts Ave., E19-411
Cambridge MA 02139-4307 (USA)

T (617) 253-7492 F (617) 253-9845
globalchange@mit.edu
http://globalchange.mit.edu

Geosci. Model Dev., 10, 2833–2848, 2017
https://doi.org/10.5194/gmd-10-2833-2017
© Author(s) 2017. This work is distributed under
the Creative Commons Attribution 3.0 License.

Geoscientific Model Development
Open Access
EGU

"Climate response functions" for the Arctic Ocean: a proposed coordinated modelling experiment

John Marshall[1], **Jeffery Scott**[1], **and Andrey Proshutinsky**[2]

[1]Department of Earth, Atmospheric and Planetary Sciences, Massachusetts Institute of Technology, 77 Massachusetts Avenue, Cambridge, MA 02139-4307, USA
[2]Woods Hole Oceanographic Institution, 266 Woods Hole Road, Woods Hole, MA 02543-1050, USA

Correspondence to: John Marshall (jmarsh@mit.edu)

Received: 23 December 2016 – Discussion started: 10 January 2017
Revised: 1 June 2017 – Accepted: 5 June 2017 – Published: 21 July 2017

Abstract. A coordinated set of Arctic modelling experiments, which explore how the Arctic responds to changes in external forcing, is proposed. Our goal is to compute and compare "climate response functions" (CRFs) – the transient response of key observable indicators such as sea-ice extent, freshwater content of the Beaufort Gyre, etc. – to abrupt "step" changes in forcing fields across a number of Arctic models. Changes in wind, freshwater sources, and inflows to the Arctic basin are considered. Convolutions of known or postulated time series of these forcing fields with their respective CRFs then yield the (linear) response of these observables. This allows the project to inform, and interface directly with, Arctic observations and observers and the climate change community. Here we outline the rationale behind such experiments and illustrate our approach in the context of a coarse-resolution model of the Arctic based on the MITgcm. We conclude by summarizing the expected benefits of such an activity and encourage other modelling groups to compute CRFs with their own models so that we might begin to document their robustness to model formulation, resolution, and parameterization.

1 Introduction

Much progress has been made in understanding the role of the ocean in climate change by computing and thinking about "climate response functions" (CRFs), i.e., perturbations to the climate induced by step changes in, for example, greenhouse gases, freshwater (FW) fluxes, or ozone concentrations (see, e.g., Good et al., 2011, 2013; Hansen et al., 2011; Marshall et al., 2014; Ferreira et al., 2015). As discussed in Hasselmann et al. (1993), for example, step function response experiments have a long history in climate science and are related to "impulse" (Green's) function responses. Here we propose a coordinated program of research in which we compute CRFs for the Arctic in response to key Arctic "switches", as indicated schematically in Fig. 1.

A successful coordinated activity has a low bar for entry, is straightforward to carry out, involves models of all kinds – low resolution, high resolution, coupled and ocean only – is exciting and interesting scientifically, connects to observations and, particularly in the context of the Arctic, to climate change and the climate change community. Our hope is that the activity set out here satisfies many of these goals. The ideas were presented to the FAMOS (Forum for Arctic Modeling and Observational Synthesis[1]) community in the autumn of 2016. This paper stems from those discussions and sets out in a more formalized way how to compute CRFs for the Arctic, what they might look like, and proposed usage. We invite Arctic modelers and observers to get involved.

The main switches for the Arctic Ocean are as follows, as indicated schematically in Fig. 1:

1. wind forcing – increasing and decreasing the wind field both within the Arctic basin (W_I) and (just) outside the basin (W_O);

2. freshwater forcing – stepping up and down the river (R) and ($E - P$) freshwater fluxes;

[1]see http://famosarctic.com

3. inflows – changes in the heat and freshwater flux, either by volume, or inflow temperature or salinity of water flowing into the Arctic Ocean from the Atlantic (A) and Pacific (B).

Each participating group would choose their preferred Arctic simulation and perturb it with exactly the same forcing fields in exactly the same manner. All other modelling choices would be left to the discretion of the individual groups. Suggested forms for, and examples of, W_I, W_O, R and A are discussed and described here. "Observables", such as the freshwater content of the Beaufort Gyre (BG), sea-ice extent etc., would be computed, with evolution maps and time series plotted and compared across the models. Differences and similarities across models will motivate scientific discussion. Convolutions with observed time series of the forcing (an example is given Sect. 3.5) allow comparisons to be made with observations (retrospectively) and climate change projections from models.

Our paper is set out as follows. In Sect. 2 we describe how we propose to compute CRFs for key observables and forcing functions in the Arctic. In Sect. 3 we illustrate the approach in the context of a coarse-resolution model of the Arctic based on the MITgcm. There we compute CRFs for the switches shown in Fig. 1 and demonstrate how convolutions can be computed for a chosen time series of the forcing from knowledge of the model response to a step. In Sect. 4 we outline a suggested protocol enabling other groups to carry out the same experiments. We conclude in Sect. 5 with a summary of expected benefits.

2 Motivation behind Arctic perturbation experiments

2.1 Response to step functions in the forcing

Much community effort goes in to building and tuning models of the Arctic that have the best possible climatology and seasonal cycle, as measured against observations. Previous coordinated experiments have compared the climate states of these models and their sensitivity to parameters and forcing fields (see, e.g., Proshutinsky et al., 2011; Ilicak et al., 2016). But one is also keenly interested in how the system responds to a *change* in the forcing, as in, for example, the idealized study of Lique et al. (2015). This is perhaps particularly true in the Arctic, which is undergoing rapid change as the Earth warms. Indeed much of climate research focuses on the change under anthropogenic forcing, rather than the mean climate. Of course fidelity in the mean might be a prerequisite for fidelity in the forced response, but this is not always the case. For example, one can make a rather good prediction of the change of global mean SST with a simple (albeit tuned) one-dimensional energy balance model which makes no attempt to capture three-dimensional dynamics. Much of the IPCC (Intergovernmental Panel on Climate Change) process concerns comparing changes in model states under forcing rather the mean states of those models.

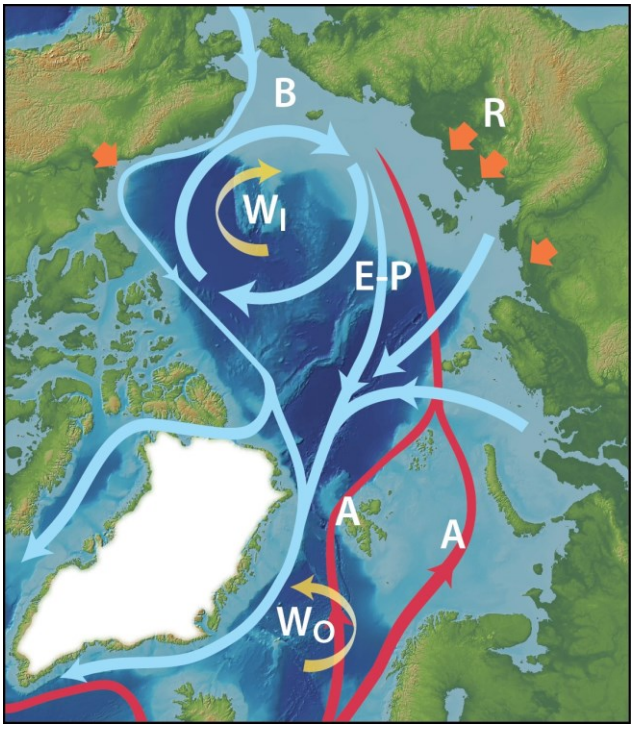

Figure 1. A schematic of circulation pathways in the Arctic Ocean and key "switches" that can perturb it. Background color coding is ocean bathymetry and elevation over land. Thick blue pathways show general branches of sea-ice drift and surface water circulation. "B" indicates the entrance of Pacific waters to the Arctic Ocean through the Bering Strait. The thin blue pathways originating in the Bering Strait region depict a hypothetical branch of Pacific water flow involved in the coastal boundary current. Red arrows represent inflows of warm Atlantic waters entering the Arctic Ocean via the Fram Strait and through the northern parts of the Kara Sea. Note that in the Fram Strait region and the Barents Sea, these branches of Atlantic water (depicted as "A") enter the Arctic Ocean and subsequently circulate around it at depths greater than 100–150 m. Key switches for the Arctic, which will be perturbed in our models, are also indicated: winds interior (W_I in the Beaufort Gyre) and exterior (W_O in the Greenland Gyre) to the Arctic basin, river runoff (R, orange arrows), evaporation − precipitation ($E - P$), and inflow of Atlantic (A) and Pacific (through the Bering Strait region B).

The coordinated experiments we are proposing here focus on the response of Arctic models to external forcing rather than comparing mean states. We organize our discussion around CRFs, i.e., the response of the Arctic to "step" changes in forcing, as represented schematically in Fig. 1, and the transient response of the system is revealed and studied.

Why step-functions? Step functions have a special status because they are the integral in time of the impulse response from which, in principle, one can construct the linear response to any time history of the forcing: if one knows

the CRF and the respective forcing function, convolving one with the other yields the predicted linear response (see, e.g., Sect. 3.5).

More precisely we may write the following (see, e.g., Marshall et al., 2014):

$$R(t) = \int_0^t \mathrm{CRF}^{\mathrm{R}}(t-t')\,\frac{\partial F}{\partial t}(t')\,\mathrm{d}t', \qquad (1)$$

where F is the prescribed forcing function (hPa, for a pressure perturbation producing anomalous winds)[2], CRF is the step response function per unit forcing, and $R(t)$ is the response. For example, R might be summertime Arctic sea-ice extent, F the wind field over the Beaufort Gyre, and CRF the response function of the ice extent to the wind. Many observables could be chosen depending on the question under study and the availability of observational time series. But it is important that they be chosen with care and represent some integral measure of Arctic response.

The "magic", then, is that if we know the response function of a diagnostic quantity to a step change in a chosen forcing, we can then convolve this response function with a time history of the forcing to obtain a prediction of the linear response to that forcing history, without having to run the actual experiment. This can be checked a posteriori by running the true experiment and comparing the predicted response to the convolution, as given in Sect. 3.5.

Finally, more support for the idea of computing the step response comes from Good et al. (2011, 2013), in which the response of climate models to abrupt $4 \times CO_2$ is used to predict global mean temperature change and ocean heat uptake under scenarios that had not been run. Gregory et al. (2015) shows how the step approach is a good way to distinguish linear and nonlinear responses in global predictions. In the same way, our project will be able to ascertain the degree of linearity of Arctic CRFs. It should be emphasized that if the system is not linear, convolutions would then provide only limited predictive skill. This may be true of, for example, Arctic sea-ice cover, given the strongly nonlinear nature of ice. One might also expect the linear assumptions to break down as the amplitude of the forcing is increased, a point to which we return below.

2.2 Choosing key Arctic forcing functions and observables

2.2.1 Forcing functions

The key switches for the Arctic Ocean are set out schematically in Fig. 1 and comprise wind anomalies both interior (W_I) to the Arctic and exterior to it (W_O), perturbations to the runoff (R), and ocean transports into the Arctic from outside (A and B). To illustrate our approach here we focus on perturbations to the wind field over the Beaufort Gyre and the Greenland Sea (GS), the heat flux through the Fram Strait, and river runoff. Many other perturbations could also be considered. Our choice of switches are motivated by the following considerations.

Wind forcing: wind is one of the most important forcing parameters driving variability of ice drift and ocean circulation ("wind blows, ice goes", a rule of thumb well known since Arctic exploration in the 17th century) and responsible for mechanical changes in sea-ice concentration and thickness, freshwater content variability, and upwelling and downwelling processes, with implications for both oceanic geochemistry and ecosystem changes.

There are two major wind-driven circulation regimes over the Arctic Ocean, namely cyclonic and anticyclonic, which have decadal variability with significant differences in environmental parameters between these regimes (Proshutinsky and Johnson, 1997; Proshutinsky et al., 2002; Thompson and Wallace, 1998; Rigor et al., 2001; Proshutinsky et al., 2015). The Beaufort Gyre and Greenland Gyre regions are key circulation cells in the central Arctic Ocean and central Nordic seas and regulated by Beaufort and Icelandic High atmospheric systems, respectively. In our recommended experiments, anomalous wind direction and intensity in these regions have been chosen, as inspired by observational data (NCAR/NCEP reanalysis products).

River runoff: river runoff is the major source of freshwater for the Arctic Ocean. The FW is a key component in the Arctic hydrological cycle, affecting ocean, sea ice, and atmosphere. In the Arctic Ocean, the FW at the surface maintains a strong stratification that prevents release of significant deep-ocean heat to the sea ice and atmosphere (i.e., halocline catastrophe; Aagaard and Carmack, 1989; Toole et al., 2010).

Arctic FW exports can affect the climate of the North Atlantic by potentially disrupting deep convection in the North Atlantic, and it can affect the Atlantic Meridional Overturning Circulation (AMOC) if Arctic freshwater reaches convective sites in the Labrador Sea (Yang et al., 2016), for example. Thus, understanding the response to river runoff (especially as the climate warms and the hydrological cycle intensifies) is important for predicting future change. Numelinn et al. (2016) and Pemberton and Nilsson (2016), for example, have found that increased river runoff leads to a strengthening of the central Arctic Ocean stratification and a warming of the halocline and Atlantic Water layers. Further, excess freshwater accumulates in the Eurasian Basin, resulting in local sea-level rise and a reduction of water exchange between the Arctic Ocean and the North Pacific and North Atlantic Oceans. Thus, we expect that our recommended experiments, with different scenarios of runoff intensity and employing a set of models with different resolutions and parameterizations, will shed light on these behaviors.

Fram Strait salt and heat fluxes: one of the fundamental aspects of the Arctic Ocean is the circulation and trans-

[2] or Sv for freshwater forcing, or PW for the heat flux anomaly associated with Arctic inflow etc.

formation of Atlantic Water, which plays a critical role in Earth's climate system. Profound modification and conversion of these waters into North Atlantic Deep Water occur within the Arctic, making this region the "headwaters" of the global meridional overturning circulation. As far back as the early 1900s, Nansen concluded that the warm intermediate layer of the Arctic Ocean originated in the North Atlantic Ocean; oceanographers have since explored the intricate pathways, behavior, and impacts of Atlantic waters throughout the Arctic basin. While we have gained an understanding and appreciation of the importance of Atlantic Water, much remains to be learned. In our recommended experiments, the heat flux through the Fram Strait is perturbed, enabling us to test a set of hypotheses about the role Atlantic waters play in the Arctic. One of them is that heat release from the Atlantic water layer is responsible for sea-ice decline in the Arctic Ocean (e.g., Carmack et al., 2015). CRF experiments will also shed light on the pathways and intensity of Atlantic water and the interaction of boundary currents with the Arctic interior.

2.2.2 Observables

Ideal observables – the left-hand side of Eq. (1) – are integrated quantities (not, for example, the temperature at one point in space), which should be constrained by observations, indicative of underlying mechanisms and of climatic relevance. Two key attributes of useful "observables" are worth emphasizing: (a) those that make reference to existing theories or hypotheses about Arctic ocean dynamics (their CRFs can then inform our understanding) and (b) those for which CRFs can be constructed from observations, providing a quantitative measure for evaluation of model skill. With regard to the latter, given the difficulty of obtaining in situ observations, our focus is on large-scale integrated quantities. Some of the best available are satellite-derived, e.g., sea-ice concentration (and ice area and extent, derived from it) and ice drift from CryoSat, freshwater content inferred from CryoSat's sea-surface height fields and sea-surface temperatures in open water areas. Ocean fluxes through straits are perhaps best constrained by in situ observations, although they suffer from a lack of near-surface observations (i.e., Woodgate et al., 2015; Beszczynska-Möller et al., 2012), especially for the freshwater flux.

The following Arctic "observables or metrics" are a useful starting point, each one of which is constrained to some degree by observations:

- freshwater and heat storage of the Beaufort Gyre;
- strength of boundary currents;
- summer and winter sea-ice extent, sea-ice thickness and volume;
- flux through various sections and straits;
- mixed layer depth;
- export of heat and freshwater to the North Atlantic Ocean.

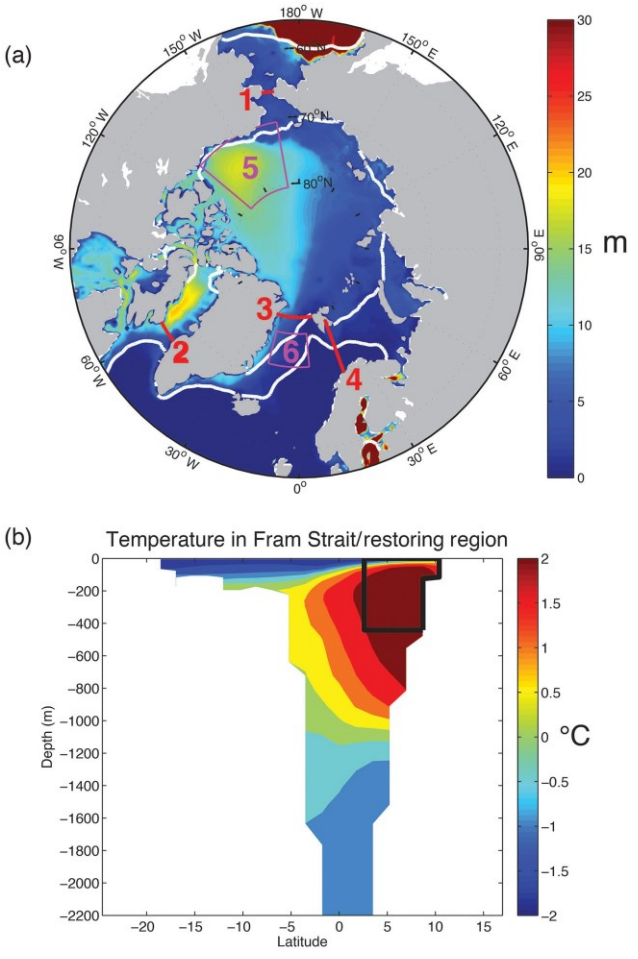

Figure 2. (a) Average FWC (freshwater content) over the period 1979–2013 (colored, in meters) from the MITgcm simulation. The summer (inner white lines) and winter sea-ice extent (outer white lines) are plotted. Key sections and regions are numbered: 1 = Bering Strait, 2 = Baffin Bay–Davis Strait, 3 = Fram Strait, 4 = Barents Sea Opening, 5 = Beaufort Gyre region, and 6 = Greenland Sea region. **(b)** Annual-mean temperature section through the Fram Strait looking northward in to the Arctic. The black box indicates the region where inflow parameters are modified in the calculations presented.

Some of the key regions and sections that are of interest to us are shown in Fig. 2. Many others are being considered.

2.3 Science questions

Key science questions are as follows:

- What sets the timescale of response of the above metrics to abrupt changes in the forcing? Some will respond

rapidly to changes in forcing, others more slowly. Can we understand why in terms of controlling physical processes?

- Are responses symmetric with respect to the sign of the perturbation? This may simply not be true in the presence of sea ice when on–off behavior can be expected. Moreover, linearity is likely to be a function of the magnitude of the applied perturbation and will likely break down if the perturbation is too large.
- Do some observables exhibit threshold behavior, or indicate the possibility of hysteresis?
- Do convolutions of the observed forcing with the CRF shed light on observed time series?

We do not have space to explore all these issues here but return to some of them in the conclusions. We now go on to present examples of the experiments we are proposing.

3 Illustrative examples with a "realistic" Arctic Ocean model

To give a concrete example of Arctic CRFs, in this section we compute the response of a coarse-resolution model of the Arctic based on the MITgcm (Marshall et al., 1997a, b; Adcroft et al., 1997) to step changes of the forcing shown in Fig. 1. We first describe the climatology of the model, the forcing functions that we use to perturb it, and the resulting CRFs, and show that they can be used to reconstruct the model's response to a time-dependent forcing.

3.1 Arctic model based on the MITgcm

3.1.1 Configuration

The simulation is integrated on the Arctic cap of a cubed-sphere grid, permitting relatively even grid spacing throughout the domain and avoiding polar singularities (Adcroft et al., 2004). The Arctic face comprises 210×192 grid cells with a mean horizontal grid spacing of 36 km. A linearised free surface is employed. There are 50 vertical levels ranging in thickness from 10 m near the surface to approximately 450 m at a maximum model depth of 6150 m. Bathymetry is from the 2004 (W. Smith, unpublished) blend of the Smith and Sandwell (1997) and the General Bathymetric Charts of the Oceans (GEBCO) 1 arc-minute bathymetric grid. The nonlinear equation of state of Jackett and McDougall (1995) is used. Vertical mixing follows Large et al. (1994) with a background diffusivity of $5.4 \times 10^{-7}\ \mathrm{m^2\,s^{-1}}$. A seventh-order monotonicity-preserving advection scheme (Daru and Tenaud, 2004) is employed and there is no explicit horizontal diffusivity. A meso-scale eddy parameterization in the spirit of Gent and McWilliams (1990) is used with the eddy diffusivity set to $K = 50\ \mathrm{m^2\,s^{-1}}$. The ocean model is coupled to a sea-ice model described in Losch et al. (2010) and Heimbach et al. (2010).

The 36 km resolution model was forced by the JRA-25 (6 h, 1°) reanalysis for the period 1979–2013, using bulk formulae following Large and Pond (1981). Initial conditions for the ocean are from the WOCE Global Hydrographic Climatology (annual-mean, 1990–1998 from Gouretski and Koltermann, 2004). Open boundary conditions on S, T, u and v were employed using "normal-year" conditions averaged from 1992–2002 derived from an ECCO climatology (Nguyen, Menemenlis and Kwok, 2011). Decadal runs take a few hours on 80 cores.[3]

3.1.2 Climatology

Our model has a reasonable climatology, as briefly illustrated in Figs. 2 and 3. Figure 2a shows a plan view of the FWC (freshwater content; see Aagaard and Carmack, 1989)[4] in the Beaufort Gyre averaged over the period 1979–2013. It has a plausible structure and is broadly in accord with, for example, Fig. 6 of Haine et al., 2015, both in magnitude and spatial pattern. The winter ice edge is marked by the "outer" white lines, the summer ice edge by the "inner" lines. Comparison with observations reveals that our modeled sea ice is rather too extensive, at both the summertime minimum and the wintertime maximum.

Time series of FWC and heat content (HC) (top 400 m) over the Beaufort Gyre (the horizontal region over which we integrate is delineated by the box in Fig. 2a) are shown in Fig. 3a and b. Figure 3a and b reveal that the freshwater and heat content are varying on decadal timescales, with an increased accumulation of FWC[5] (by roughly 2500 $\mathrm{km^3}$) in the 2000s and a leveling out in heat content relative to earlier decades. The recent trends (on the order of 10 % of the mean) may have been associated with an increased anticyclonic wind over the BG (Proshutinsky et al., 2009; Rabe et al., 2014). The evidence is reviewed in Haine et al. (2015).

[3] Very similar 18 and 4 km configurations of the same model exist and can be used in eddy permitting simulations for comparison with the coarse model run shown here.

[4] Freshwater content is defined here (as reviewed in Haine et al., 2015) as the amount of zero-salinity water required to reach the observed salinity in a seawater sample starting from a reference salinity. It is computed as follows: $\mathrm{FWC} = \int_D^{\eta} \frac{S_{\mathrm{ref}} - S}{S_{\mathrm{ref}}}\,\mathrm{d}z$, where η is the free surface and we choose $S_{\mathrm{ref}} = 34.80$ and D is its depth. This is the quantity mapped in Fig. 2a. Similarly, freshwater flux (FWF) is defined by multiplying the integrand of the above expression by velocity and integrating along the section.

[5] To convert the FWC of the BG to meters of freshwater, divide by the surface area of the BG, here taken to be $1.24 \times 10^6\ \mathrm{km^2}$, the area of the box in Fig. 2a. Thus a FWC $= 20 \times 10^3\ \mathrm{km^3}$ corresponds to a depth of $\frac{20 \times 10^3\ \mathrm{km^3}}{1.24 \times 10^6\ \mathrm{km^2}} = 16$ m of freshwater.

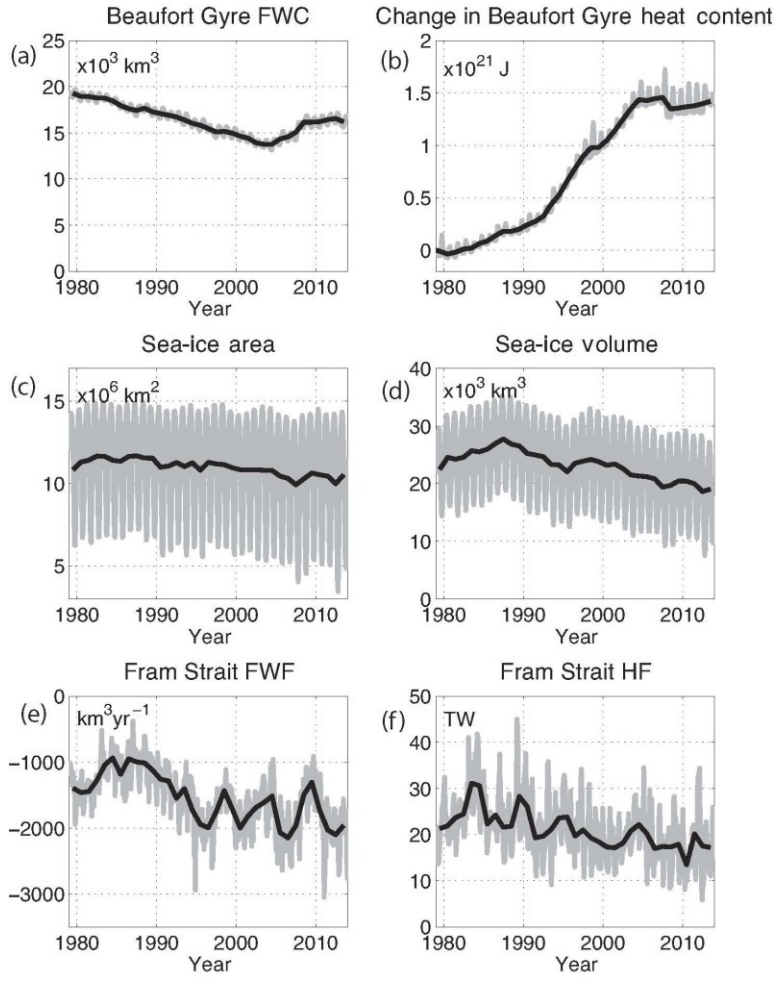

Figure 3. Time series of **(a)** freshwater content (FWC) and **(b)** heat content (HC) of the BG, **(c)** sea-ice area and **(d)** sea-ice volume over the Arctic, **(e)** freshwater flux (FWF, negative values imply a flux out of the Arctic), and **(f)** heat flux through the Fram Strait (HF, positive values indicate a flux in to the Arctic). The thick black line plots annual-mean values; the grey line tracks monthly means. Note that the units of the *y* axis appear in the top-left-hand corner of each panel.

It is also clear from Fig. 3 that the model is drifting with a downward (upward) trend in FWC (HC). The model described here has undergone no data-assimilative procedure and so might be expected to exhibit such drifts as it adjusts to the initial conditions and forcing.

Figure 3c plots the annual cycle of sea-ice area from the 1980s onwards, showing a decline in the minimum (summer) ice area on the order of 10^6 km^2 in 30 years. The observed rate of sea-ice extent loss is much more dramatic than captured in our model: observations suggest that sea ice has declined by $\sim 0.5 \times 10^6$ km^2 per decade (annual mean) in the last few decades to below 8×10^6 km^2 (see, e.g., Fig. 1a of Proshutinsky et al., 2015), whereas the modeled annual-mean area is 11×10^6 km^2.

Figure 2b shows a vertical temperature section through our model, roughly coinciding with the Fram Strait (as indicated in Fig. 2a), and Fig. 3e–f plot time series of FWF (freshwater flux) and HF (heat flux) through the strait: positive indicates a flux into the Arctic, negative out of the Arctic. We observe a strong seasonal cycle and much interannual variability superimposed on longer-term trends and/or drifts. The magnitude of the mean value of FWF is somewhat smaller than the 2700 ± 530 km^3 yr^{-1} estimated from observations (see Table 1 and Fig. 4 of Haine et al., 2015). The HF through the Fram Strait varies by $\sim$ 10TW over the period of our simulation, roughly comparable with the CORE ocean models reported in Ilicak et al. (2016).

In Fig. 4 we plot time series of annual-mean anomalous heat flux through various Arctic straits shown in Fig. 2a. We observe, for example, that heat transport through the Barents Sea strait seems to be increasing and that through the Fram Strait is decreasing with a decadal trend. In contrast the transport through the Bering Strait and Baffin Bay vary primarily on interannual timescales, with less evidence of decadal trends. Comparison of the time series shown in Fig. 4 with those in Figs. 11 through 14 of Ilicak et al. (2016) shows

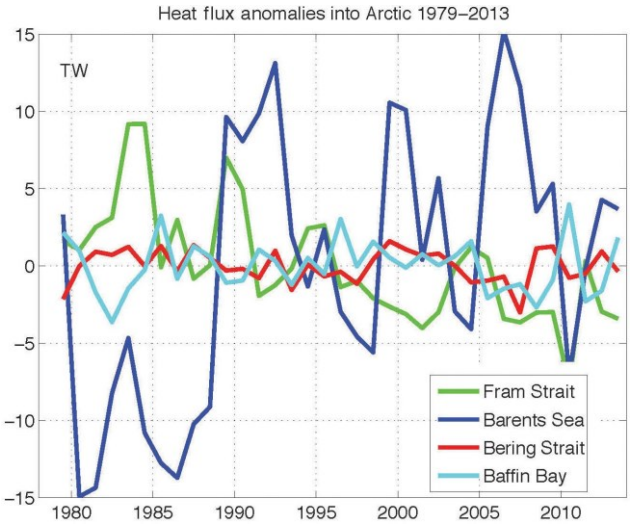

Figure 4. Heat flux anomalies (seasonal cycle removed) across key Arctic straits, as indicated in Fig. 2. The units are of the *y* axis are terawatts (TW).

broad similarities despite the fact that the latter study uses CORE forcing and a variety of models employing differing physical parameterizations, open boundary conditions, and grid resolutions.

It is clear from the above brief review of key circulation and sea-ice metrics (clearly many more are likely to be of interest) that they respond to the various external drivers in different ways with respect to amplitude and timescale. As we now go on to describe, we can expose and explore some of the underlying mechanisms by computing how the model responds to a step increase in the forcing.

3.2 Anomalies in forcing functions

We now describe the prescription of the forcing function anomalies in wind, river runoff, and transport through the straits.

3.2.1 Wind

Simplified forms of the surface pressure anomalies over the Beaufort Gyre and Greenland Sea have been constructed and are plotted in Fig. 5. The center for the BG pressure anomaly is located at 77° N, 149° W and the center for the GS anomaly is located at 71° N, 6° W, with a radius of influence on the order of 1000 km. The magnitude of the anomaly is the same for all experiments. Our choice of BG and GS atmospheric centers of action were identified based on 1948–2015 6 hourly NCAR/NCEP data. These data were analyzed to identify key locations of centers of action and typical magnitudes north of the Arctic Circle. These centers can also be determined from Thompson and Wallace's (1998, 2001) studies of the Arctic Oscillation (AO, first mode of SLP EOF analysis which describes approximately 19 % of SLP variability in December–March).

In the series of experiments described here we assumed a central maximum/minimum of 4 hPa. Our perturbation of 4 hPa is small relative to seasonal changes, which can reach 20–30 hPa. However, a more reasonable measure is to compare with longer-term trends. During the 1948–2015 period, SLP over the Arctic changed by about 6 hPa suggesting that our chosen magnitude is not unrealistic. As can be seen by inspection of the right hand panels of Fig. 5, there is a noticeable perturbation to the long-term climatology of SLP when anomalies of this magnitude are assumed.

To compute surface winds from these pressure anomalies, the following relation is used (Proshutinsky and Johnson, 1997):

$$W_s = 0.7 \times \begin{vmatrix} \cos 30 & -\sin 30 \\ \sin 30 & \cos 30 \end{vmatrix} \times W_g$$

where W_g is geostrophic wind implied by the pressure anomaly, and W_s is the applied surface wind anomaly. The resulting anomalous winds are also plotted in Fig. 5.

3.2.2 Fluxes through straits

We perturb the properties of water masses flowing through the Fram Strait. For simplicity we aligned the section with our model grid, extending from grid points centered at 80° N, 10° E (near Svalbard) to 80° N, 19° W (the Greenland coast), marking a line close to a true parallel (see Fig. 2a). Our objective is to perturb the temperature of water flowing across the section into the Arctic, but without a concomitant density change. This is accomplished by rapid restoration of temperature while simultaneously restoring salt to compensate. In the experiments described here, the restoring temperature was $T + 2$ K and restoring salinity was $S + 0.253$ psu[6], where both T and S were monthly fields diagnosed from our 35-year control run. The restoring area was limited both in zonal extent and depth along the section: from 80° N, 10° E (Svalbard coast) to 80° N, 3.5° E, in the vertical from the surface to 440 m, as indicated by the box in Fig. 2b. The box was chosen to capture the main core of Atlantic water entering the Arctic through the strait. A restoring time constant of 9 days was used for both T and S. This simple procedure ensures that the potential density in the Fram Strait section in the control and the forced experiment are very similar.

3.2.3 Runoff

For the anomalous river runoff experiment (RUN3x), the freshwater input from all rivers which drain into the ocean

[6]Compensating for salinity, $\delta S = \frac{\alpha}{\beta}\delta T = 0.253$ psu, was computed using a $\delta T = 2$ K assuming $\alpha = 1 \times 10^{-4}$ K^{-1} and $\beta = 7.9 \times 10^{-4}$ psu^{-1}, roughly corresponding to 5 K and 33 psu seawater, respectively.

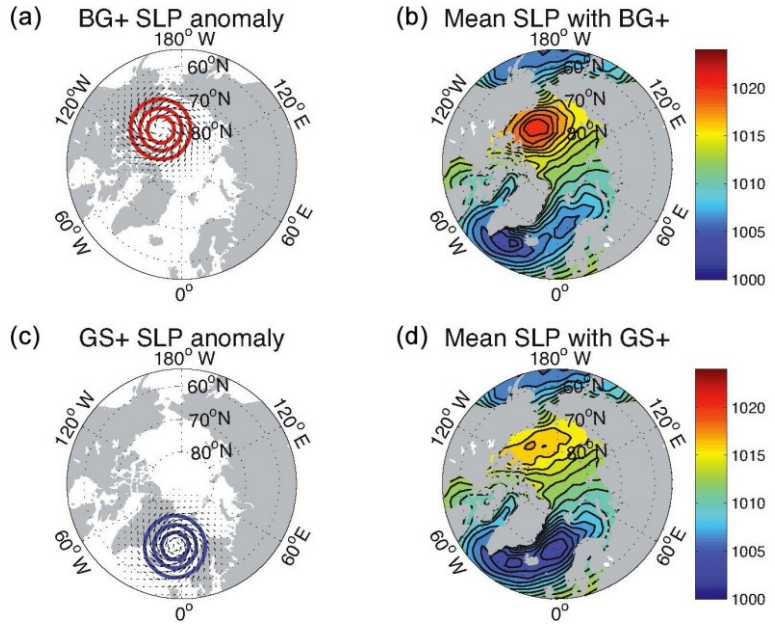

Figure 5. (a) Idealized sea-level pressure anomaly of 4 hPa and associated winds constructed for the Beaufort Gyre (BG). Note that the BG*(+)* corresponds to anomalously high pressure. **(b)** BG*(+)* SLP anomaly added to the NCEP 1981–2010 SLP climatology. **(c)** Idealized sea-level pressure anomaly of 4 hPa and associated winds constructed for the Greenland Sea (GS). Note the GS*(+)* corresponds to anomalously low pressure over the GS. **(d)** GS SLP anomaly added to the 1981–2010 SLP climatology. The contour interval in **(a)**–**(d)** is 1 hPa.

north of the Arctic Circle (66° N) was multiplied by a factor of 3. In our regional Arctic setup, no effort was made to balance this anomalous freshwater input with additional evaporation.

3.3 Climate response functions

Figures 6–8 show the CRFs for, respectively, the BG wind anomaly, the GS wind anomaly, and the runoff and Fram Strait temperature anomaly. The forcing anomalies are applied one at a time, although combinations would also be of interest. We focus on metrics of FWC, HC, sea-ice area and volume, and Fram Strait FWF and HF. This is an interesting subset of the large number of circulation and ice metrics that could be computed and discussed. There are interesting spatial patterns of response but they are not discussed here.

In Fig. 6 the CRFs of key quantities for the positive *(+)* and negative *(−)* BG wind anomalies are shown. The + sign indicates that the Beaufort High is anomalously strong, with enhanced anticyclonic flow. We see that in response to anomalously high surface pressure over the BG, its FWC increases, readjusting to a new quasi-equilibrium after about 30 years but continuing to trend upward. An increase in FWC is to be expected since enhanced anticyclonic winds and their associated Ekman transport draw freshwater from the periphery of the BG, increasing its FWC. As the BG freshens it also becomes colder, as seen by its decreasing heat content (Fig. 6b). Thus freshwater and temperature changes tend to compensate for one another with respect to their effect on density. We see from Fig. 6c that there is little change in the sea-ice area in response to the enhancement of the anticyclonic wind field, but a substantial increase in the volume of sea ice: evidently sea ice is converging and thickening.

In Fig. 7 the CRFs of key quantities for the positive and negative GS wind anomalies are shown. Note that a positive sign indicates that the low-pressure system that resides over the GS (the northward extension of the Icelandic Low) is anomalously strong, thus inducing anomalously cyclonic circulation over the Barents and Greenland seas – see Fig. 5b. In response to GS*(+)*(GS*(−)*) the BG FWC increases (decreases) slightly, but with a delay of 10 years or so. This is presumably an advective signal. There is a pronounced change (but again with a decadal delay) in the HC of the BC, which warms in the negative case and cools in the positive case. Unlike for the BG wind forcing, we observe a notable increase in sea-ice area for a negative anomaly and a decrease for a positive anomaly. An increase in low pressure over the GS leads to increased advection of sea ice out of the Arctic through the Fram Strait and advection of warm water into the Arctic, resulting in ice melt: both factors lead to a decrease in sea-ice area. Changes in sea-ice volume are also observed but with reduced magnitude relative to the BG wind anomalies. CRFs for Fram Strait FWF and HF induced by GS wind anomalies are all suggestive of a two-timescale process at work – with the response changing sign after 10 years or so

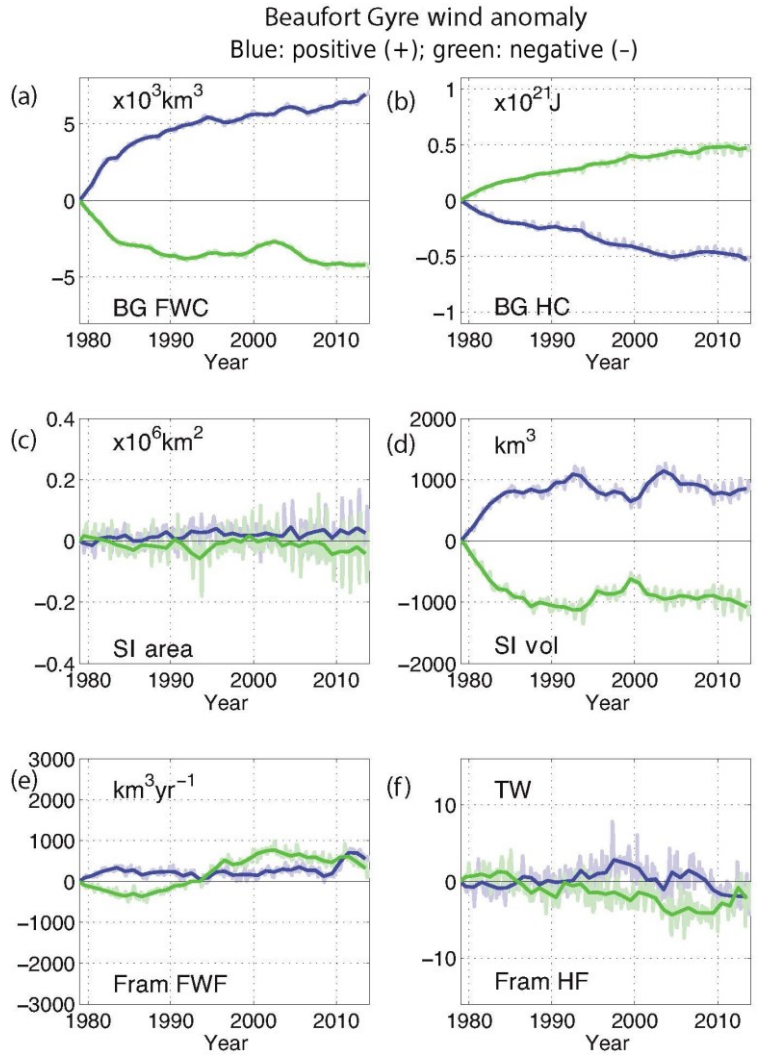

Figure 6. CRFs for the Beaufort Gyre wind anomaly, blue *(+)* and green *(−)*. Note that the + sign implies a stronger anti-cyclonic forcing. The response to a 4 hPa surface pressure anomaly (see Fig. 5a) is shown of **(a)** $C^{W_{BG}}_{FWC_{BG}}$, the FWC of the BG **(b)** $C^{W_{BG}}_{HC_{BG}}$, HC of the BG **(c)** $C^{W_{BG}}_{SIA}$, SI area **(d)** $C^{W_{BG}}_{SIV}$, SI volume **(e)** $C^{W_{BG}}_{FWF_{Fram}}$, FWF through the Fram Strait and **(f)** $C^{W_{BG}}_{HF_{Fram}}$, the HF through the Fram Strait. Note that the units of the *y* axis appear in the top-left-hand corner of each panel.

in the case of the Fram FWF and after 5 years or so in the case of the Fram HF.

Figure 8 shows the response of our key metrics to changes in runoff and Fram Strait heat transport implemented, as described in Sects. 3.2.2 and 3.2.3. It should be noted that these are rather large perturbations, much greater than might be expected to occur naturally. We see that as runoff is increased, the southward FWF through the Fram Strait increases linearly over a 30-year period with a compensating northward heat flux, and the FWC of the BG increases very slightly, as does sea-ice area and volume. An impulsive increase in the HF through the Fram Strait leads to an increase in the HC of the BG after a decade or so but has no discernible effect on the other metrics under consideration.

Some of our results can be compared with findings of Nummelin et al. (2015, 2016) and Pemberton and Nilsson (2016), who studied the impact of river discharge on the Arctic Ocean. These studies assumed that future Arctic river runoff will likely increase due to intensification of the global hydrological cycle. One interesting finding of the latter study was that under an increased freshwater supply, the Beaufort Gyre weakens and there is increased freshwater exported through the Fram Strait. Here, FWC of the BG is indeed insensitive to runoff (Fig. 8a) and instead results in increased freshwater flux through the Fram Strait (Fig. 8e). Narrow fresh coastal flows can explain the insensitivity of BG FWC to the increased river runoff. Evidently most of the freshwa-

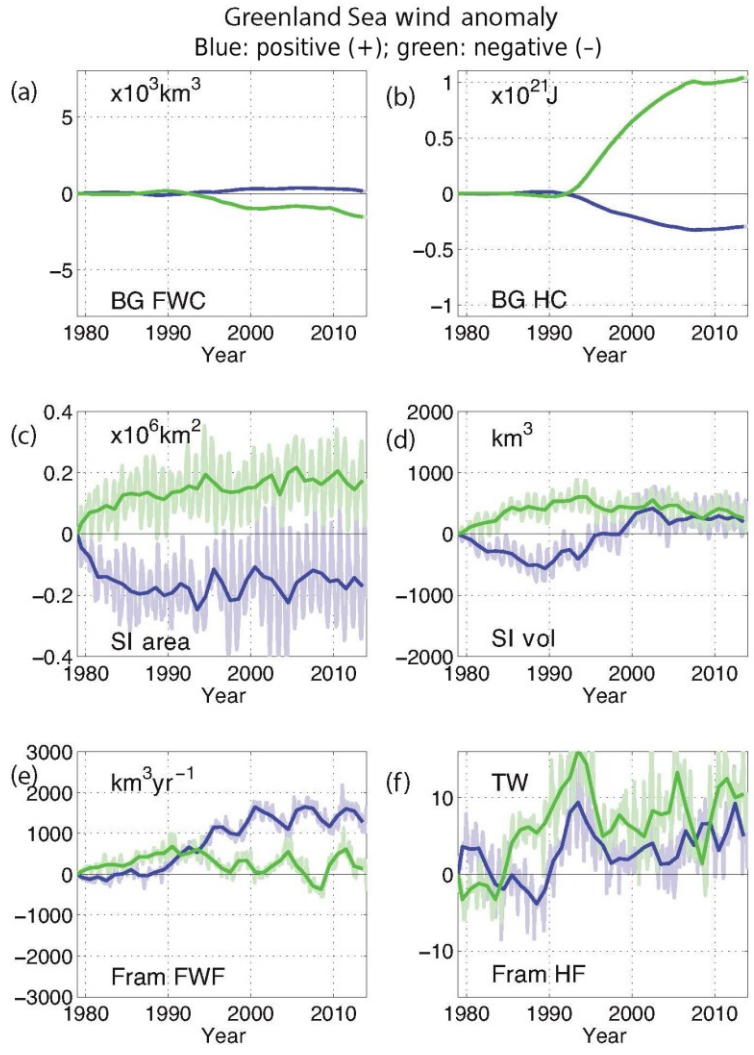

Figure 7. CRFs for the Greenland Sea wind anomaly, blue *(+)* and green *(−)*. Note that the + sign implies a stronger cyclonic forcing. The response to a 4 hPa surface pressure anomaly (see Fig. 5b) is shown of **(a)** $C^{W_{GS}}_{FWC_{BG}}$, the FWC of the BG **(b)** $C^{W_{GS}}_{HC_{BG}}$, HC of the BG **(c)** $C^{W_{GS}}_{SIA}$, SI area **(d)** $C^{W_{GS}}_{SIV}$, SI volume **(e)** $C^{W_{GS}}_{FWF_{Fram}}$, FWF through the Fram Strait and **(f)** $C^{W_{GS}}_{HF_{Fram}}$, the HF through the Fram Strait. Note that the units of the *y* axis appear in the top-left-hand corner of each panel.

ter is transported directly to the Fram and Canadian straits rather than being accumulated in the BG region.

In summary, the following general features of the CRFs are worth noting:

1. The CRFs do not respond immediately to a step in the forcing, but adjust over time, on a timescale that depends on the metric and the forcing being considered.
2. Some CRFs (e.g., FWC) have a simple form that can be characterized by a single timescale. Others are suggestive of a two timescales and/or zero-crossing (change of sign) behavior (eg. Fram Strait HF and FWF).
3. The CRFs are (roughly, but not all) symmetric with respect to a change in the sign of the forcing, as one would expect if the behavior were linear. Note, however, that as the amplitude of the forcing is increased to rather unrealistic levels, asymmetries in the response become more prevalent (not discussed further here).

3.4 Ensembles

To test the robustness of our CRFs we generate an ensemble by varying the time of onset of the forcing step function. In Fig. 9, we show the CRFs for (a) the FWC in the Beaufort Gyre (b) and the heat transport through the Fram Strait, varying the start time of the BG+ wind anomaly step function to day 1 of each month over the run's first year. We see that the FWC CRF shows minimal response to varying the seasonal timing of the forcing anomaly. This is not surpris-

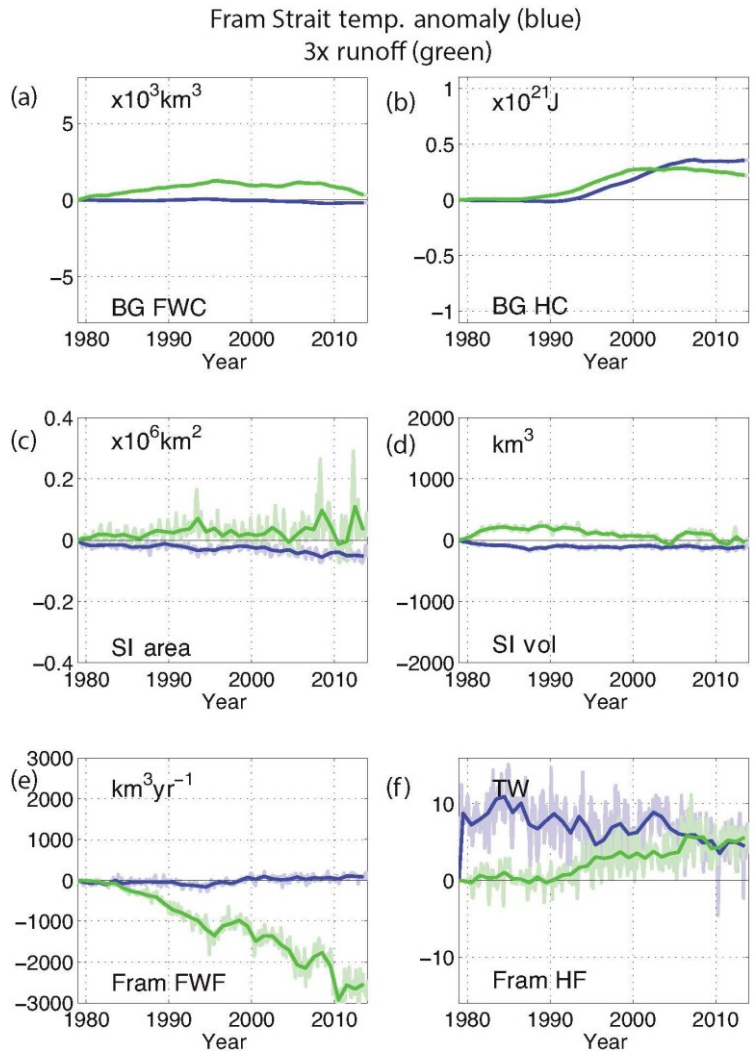

Figure 8. CRFs in response to an impulsive 3× Runoff (green lines) and Fram Strait T (+2C) anomaly (blue lines): **(a)** the FWC of the BG **(b)** HC of the BG **(c)** SI area **(d)** SI volume **(e)** FWF through the Fram Strait, and **(f)** the HF through the Fram Strait. Note that the units of the y axis appear in the top-left-hand corner of each panel.

ing given that FWC is an integrated quantity over the upper ocean salinity field. Conversely, the heat flux through the Fram Strait shows a much larger envelope in the collective ensemble CRF, yet maintains the same basic form. It will be useful to compare similarly generated ensembles across other models for these and other model metrics. Our calculations suggest that not many ensemble members – perhaps five – will be required, at least in coarse-resolution models such as the one used here.

3.5 Convolutions

Having described the form of some key CRFs, we now convolve them with periodic forcing functions to compute the implied linear response of, for example, an oscillating wind anomaly. This is then compared to direct calculations with our full ocean model to provide a sanity check on our methodology and the utility of CRFs. To make things concrete we will focus on the FWC of the BG and wind anomalies over the BG.

We adopt the following nomenclature and define $C^{W_{\mathrm{BG}}}_{\mathrm{FWC_{BG}}}$ ($\mathrm{m^3\ hPa^{-1}}$) here as the response function per unit forcing of the FWC of the BG induced by pressure anomalies (and their associated winds) over the BG, $\mathrm{FWC_{BG}}$ ($\mathrm{m^3}$) is the FWC of the BG, and W_{BG} (hPa) is the pressure anomaly over the BG. We may specialize Eq. (1) to consider the evolution of the FWC of the BG:

$$\mathrm{FWC_{BG}}(t) = \int_0^t C^{W_{\mathrm{BG}}}_{\mathrm{FWC_{BG}}}{}^{\mathrm{R}}(t-t')\ \frac{\partial W_{\mathrm{BG}}}{\partial t}^{\mathrm{R}}(t')\ \mathrm{d}t', \qquad (2)$$

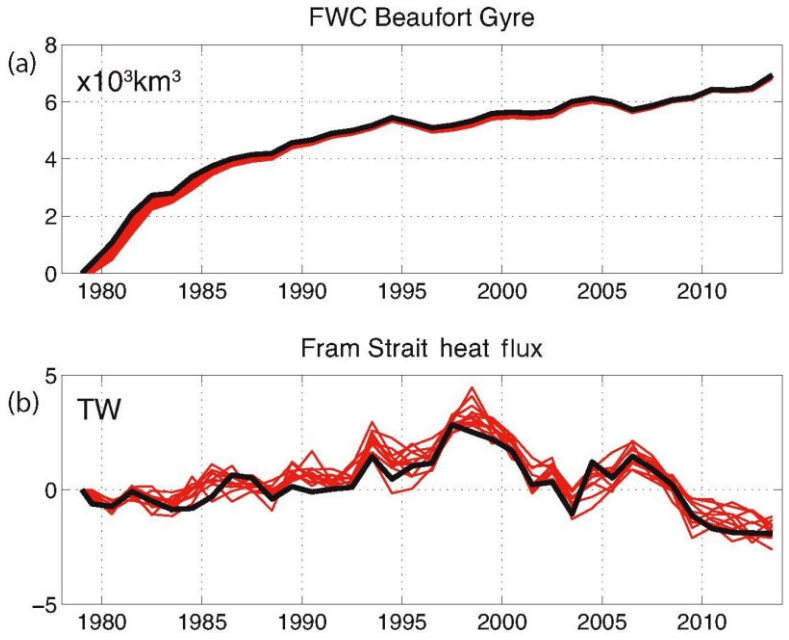

Figure 9. CRFs for the BG(+) wind anomaly for **(a)** the BG FWC and **(b)** heat flux through the Fram Strait (seasonal cycle removed). The thick black curve is the CRF with the forcing step function anomaly applied on 1 January 1979; ensemble members are show as thin red curves, with the forcing step function applied on 1 February, 1 March, . . ., 1 December 1979. Note that the units of the y axis appear in the top-left-hand corner of each panel.

where W_{BG} is the prescribed forcing anomaly (hPa, for the pressure anomaly over the BG).

Imagine now that the BG surface pressure anomaly has oscillatory form as follows:

$$W_{BG} = \hat{W}_{BG} \sin \omega t, \tag{3}$$

where $\hat{W}_{BG}$ is the amplitude of the surface pressure anomaly (hPa) and ω is the frequency on which it varies. Let us fit an analytical expression to the FWC BG response function. As can be seen in Fig. 6a, it rises on decadal timescales toward a new equilibrium after 30 years or so, but continues to slowly drift upwards. The response to a negative perturbation is (roughly) of opposite sign. The following analytical expression broadly captures the form of $C^{W_{BG}}_{FWC_{BG}}$:

$$C^{W_{BG}}_{FWC_{BG}} \times W_{BG_{step}} = \hat{F}WC_{BG}(1 - \exp(-\gamma t)), \tag{4}$$

where the scaling factor $W_{BG_{step}}$ is the magnitude of the step function in the forcing used to construct the CRF and $\hat{F}WC_{BG}$ is the amplitude of the resulting change in the FWC of the BG. The coefficients $\hat{F}WC_{BG}$ and γ depend on the nature of the forcing and the metric under consideration. They are obtained by fitting the analytical form to the curves shown in the Fig. 6a.[7]

The FWC of the BG in response to a forcing can then be written, using Eqs. (2), (3), and (4), and evaluating the following integral:

$$\begin{aligned} FWC_{BG}(t) &= \frac{\hat{W}_{BG}}{W_{BG_{step}}} \hat{F}WC_{BG} \\ &\times \int_0^t 1 - \exp -\gamma (t - t') \, \omega \cos \omega t' \, dt' \\ &= \frac{\hat{W}_{BG}}{W_{BG_{step}}} \left(\frac{\hat{F}WC_{BG}}{1 + \frac{\omega^2}{\gamma^2}} \right) \sin \omega t - \frac{\omega}{\gamma} \cos \omega t - e^{-\gamma t} . \end{aligned} \tag{5}$$

There are some interesting limit cases:

1. For times much longer than γ^{-1}, the exponential term dies away and the response oscillates at constant amplitude but shifts in phase relative to the forcing.

2. If $\frac{\omega}{\gamma} \ll 1$ (low-frequency winds) then the response is in phase with the forcing and has an amplitude $\frac{\hat{W}_{BG}}{W_{BG_{step}}} \hat{F}WC_{BG}$.

[7] Exponential CRFs are obtained for classical dynamical systems linearized about an equilibrium governed by $\frac{dY}{dt} = -\gamma Y + F(t)$, where Y is the CRF and F is the forcing, yielding a solution $Y = \frac{F}{\gamma}(1 - e^{-\gamma t})$. The parameter γ can be interpreted as a stability parameter characterizing the system which, if linear, is independent of the amplitude of the forcing. See a discussion of γ in Manucharyan et al. (2016).

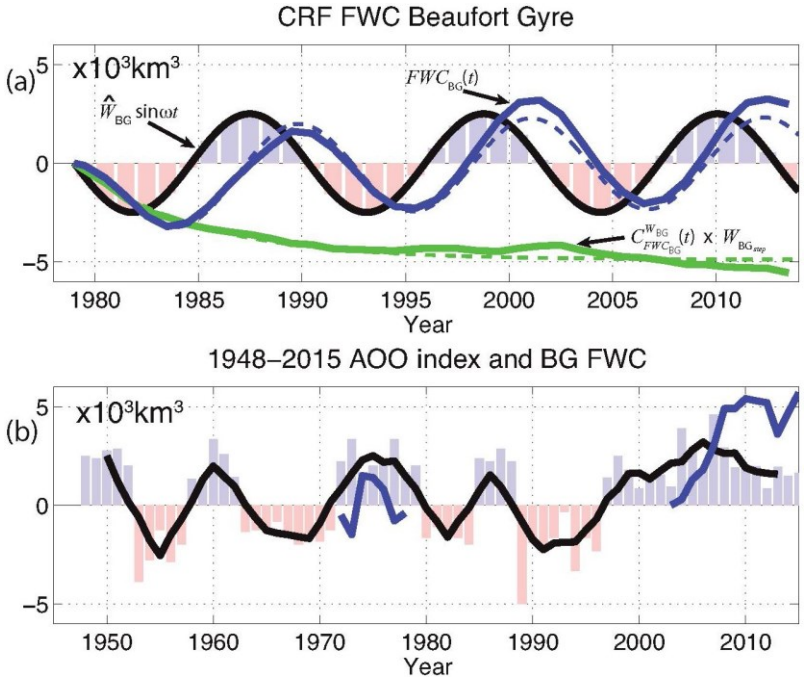

Figure 10. (a) Analytical solution (Eq. 5) for the response of the FWC of the BG (blue dashed line) to a sinusoidal wind W_{BG} of the form Eq. (3) (thick black line) assuming a response function of the form Eq. (4) (green dashed line is a fit to the thick green line which itself is the average of the (abs) plus and minus CRFs from Fig. 6a, plotted as the minus response). The response of the Arctic GCM to the sinusoidal wind forcing is plotted in the same manner in the thick blue line for comparison. **(b)** The (nondimensional) AOO, an index measuring the intensity of the Beaufort High (bars and thick black line), from 1948–2015 (see Proshutinsky et al., 2015). All lines are 5-year running means. A positive index corresponds to years with an anticyclonic wind stress over the BG, and a negative index is years with a cyclonic wind stress over the BG. The blue line shows observed anomalies of freshwater content (thousands of cubic kilometers) in the BG region. Note that the units of the *y* axis appear in the top-left-hand corner of each panel.

3. If $\frac{\omega}{\gamma} \gg 1$ (high-frequency winds) then the response is 90° out of phase with the forcing with a much diminished amplitude of $\frac{\gamma}{\omega}\frac{W_{BG}}{W_{BGstep}}FWC_{BG}$.

Let us now insert some typical numerical values. Fitting curves to $C^{W_{BG}}_{FWC_{BG}}$ (Fig. 6a) suggests that $\gamma = \frac{1}{5.7}\,\mathrm{yr}^{-1}$ with FWC$_{BG} = 4.9 \times 10^3$ km^3 (the thick green line in Fig. 6a is the average of the (abs) – absolute value – plus and minus CRFs plotted as the negative response). We suppose that the Beaufort High oscillates with an amplitude of $W_{BG} = 6.3$ hPa, changing in sign with a period of 11 years or so, broadly in accord with observations reported in Proshutinsky et al. (2015) (see Fig. 10b). Then $\omega = \frac{2\pi}{11\,\mathrm{yr}} = 0.57\,\mathrm{yr}^{-1}$ and $\frac{\omega}{\gamma} = \frac{0.57}{(1/5.7)} = 3.25{,}21$. This suggests that one would expect to see a 90° phase lag between the response of the FWC of the BG relative to that of the forcing at these periods with, after the transient has died out, an amplitude of $\frac{\gamma}{\omega}\frac{W_{BG}}{W_{BGstep}}FWC_{BG} = 2.26 \times 10^3$ km^3. The solution, Eq. (5), is plotted in Fig. 10a, along with the response function and the wind field so that one can readily ascertain the phase of the response relative to the forcing. In the first cycle $W_{BG} < 0$ and FWC$_{BG}$ decreases, but lags the forcing by 90°, or 2.75 years if the period of the forcing is 11 years. Our analytical prediction (dashed blue line) compares very favorably to that obtained by direct numerical simulation (thick blue line) in which an oscillating BG wind perturbation was applied to the GCM. This lends strong support to the utility of our approach and the merit of computing CRFs. We now briefly discuss the implications of these results for the observational record of wind forcing and FWC over the BG.

3.5.1 Implications for our understanding of decadal variations in the FWC of the Beaufort Gyre

The framework we have set up can be used to help us understand how the FWC of the BG has varied over the past few decades. Comparing Figs. 6a, 7a, and 8a, we see that wind anomalies in the GS region and perturbations to runoff do not significantly affect FWC$_{BG}$ when compared to changes in the local wind field over the BG. Moreover, if the wind field over the BG oscillates on timescales shorter than the equilibration timescale of the FWC response function, then the FWC will not be in phase with variations in the wind but instead will lag it in time.

Figure 10b plots an index of the BG high (the AOO, the Arctic Ocean Oscillation Index, a measure of the wind-stress

curl integrated over the BG) from 1948 up until 2015 – see Proshutinsky et al., 2015, and the legend therein for more details – which oscillates over a period of 11 years or so, as assumed in the analytical solutions shown in Fig. 10a. Also plotted is the FWC from observations from a short period in the 1970s and continued on from 2003. From the early 1990s up until the mid 2000s the anticyclonic driving (as measured by the AOO) over the BG markedly increased. In 2007, the Beaufort High reached a maximum because very strong anticyclonic winds dominated over the gyre throughout the year, decaying in later years. The observed FWC, however, lags the forcing and continues to build, not unlike the prediction obtained from our analytical forcing, plotted in Fig. 10a for comparison. One can see that the maximum FWC is observed approximately 3 years after maximum forcing. Of course this is only suggestive – given the short observational record it is impossible to quantitatively check the correctness of the predicted 90° lag ($\sim$ 3 years) between forcing and the BG FWC response to it. Note, for example, that the short observational record in the mid-1970s appears to be in phase with the forcing. That said, it is very unlikely that the FWC can immediately come into equilibrium with the forcing and is much more likely to exhibit a lagged response to the wind, as hinted at in the longer observational record starting in 2003 (shown in Fig. 10b).

What is the physics behind the FWC response function setting the timescale γ^{-1}? At least three important mechanisms come to mind. Firstly the wind-stress curl pumps water down from the surface, inflating the freshwater layer. But this occurs in the presence of ice whose ability to communicate the wind stress to the fluid column beneath depends on the nature of the ice pack – a difficult process to model. Perhaps sea-ice dynamics are fast relative to γ^{-1}, whereas slower sea-ice thermodynamical processes play more of a role in the CRF timescale. Secondly, baroclinic instability of the BG may be an important mechanism that spreads the FW away laterally, allowing an equilibrium to be achieved (Manucharyan and Spall, 2016; Manucharyan et al., 2016). The timescale and equilibrium level at which this is achieved depends on the eddy field which is imperfectly modeled and/or parameterized. Thirdly, the availability of freshwater sources and timescales associated with its modification by mixing near continental shelves may come in to play. Thus there is uncertainty in γ and $\mathrm{FWC}_{\mathrm{BG}}$, which controls the detailed response.

4 Protocol of proposed perturbation experiments

It would be very interesting to determine how robust the response functions shown in Figs. 6–8 are across models and understand their dependencies on resolution and physical parameterisation, for example. The CRFs described here are important because, as we have demonstrated, they control and are a summary statement of the response of key Arctic metrics to external forcing. We therefore encourage other groups to carry out such calculations so that we can compare CRFs across many models. Groups would choose their "best" Arctic simulation (by comparing to observed variables: ice thickness, ice extent, freshwater content, Atlantic water circulation, and ability to capture dominant halocline parameters and Arctic water masses) and perturb it in the manner described in Sect. 3. The forcings would be identical in all models participating in the CRF experiments. They are available from the authors, along with recommended protocols for carrying out the experiments, and can be downloaded from the web, as described at the end of the paper. 30-year runs would be required with five ensemble members spawned from perturbed initial conditions or by varying the onset timing of the forcing step function. Monthly means of T, S, currents, sea-ice concentration, and thickness would be stored and used to compute CRFs. A more detailed account of recommended data output and required model descriptions is also available.

5 Conclusions and expected benefits

Here we have introduced the idea behind and given illustrative examples of Arctic CRFs. They provide a summary statement of how the Arctic responds to the key switches shown in Fig. 1. An Arctic model comparison project with CRFs as the organizing theme could have many benefits. A focus on the transient response of Arctic models is of direct relevance to Arctic climate change, enabling us to engage and overlap with the climate change community. Moreover, the framework would enable the project to be informed by, and inform, observations over recent decades and attempts to constrain CRFs by observations would be very profitable. Many different kinds of models could be engaged including ocean-only, coupled, coarse-resolution, and eddying models, as well as models with different formulations and physical parameterizations. By doing so the robustness, or otherwise, of CRFs could be determined across a wide range of models and allow different forcing mechanisms to be ranked in order of importance. The "physics" behind the form of the CRFs would become a natural theme, likely leading to insights into mechanisms underlying Arctic climate change and allowing us to connect to idealized conceptual modelling and theory. In this way the analysis of CRFs can help in the quantitative evaluation of existing hypotheses about Arctic ocean and ice dynamics.

Finally, CRFs could become the building blocks of a physically based forecast system for the Arctic which harnesses the input of many models to refine the response functions.

Code availability. The MITgcm is an open source code that can be found online here: http://mitgcm.org/. The 36 km Arctic regional model used here is available for public

download: http://wwwcvs.mitgcm.org/viewvc/MITgcm/MITgcm_contrib/arctic/cs_36km/. The code version used in these experiments was checkpoint 65s.

Data availability. A PDF giving protocol instructions, together with netcdf files containing the forcing fields used in the CRF experiments, can be found here: http://svante.mit.edu/~jscott/FAMOS/Arctic_CRF_Protocol.pdf.

Competing interests. The authors declare that they have no conflict of interest.

Acknowledgements. The experiments described here were made possible by support from the NSF program in Arctic Research, award number 1603557. Jeffery Scott received support from the Joint Program on the Science and Policy of Global Change, which is funded by a number of federal agencies and a consortium of industrial and foundation sponsors. For a complete list please visit http://globalchange.mit.edu/sponsors. The comments of Georgy Manucharyan and an anonymous reviewer are gratefully acknowledged, as are the comments of the GMD Editor, Sophie Valcke. We would also like to thank the whole FAMOS community, who advised us and lent their support to this effort.

Edited by: Sophie Valcke
Reviewed by: Georgy Manucharyan and one anonymous referee

References

Aagaard, K. and Carmack, E.: The role of sea ice and other fresh water in the Arctic circulation, J. Geophys. Res., 94, 14485–14498, https://doi.org/10.1029/JC094iC10p14485, 1989.

Adcroft, A. J., Hill, C. N., and Marshall, J.: Representation of topography by shaved cells in a height coordinate ocean model, Mon. Weather Rev., 125, 2293–2315, https://doi.org/10.1175/1520-0493%281997%29125%3C2293:ROTBSC%3E2.0.CO;2, 1979.

Adcroft, A., Campin, J.-M., Hill, C., and Marshall, J.: Implementation of an atmosphere-ocean general circulation model on the expanded spherical cube, Mon. Weather Rev., 132, 2845–2863, https://doi.org/10.1175/MWR2823.1, 2004.

Beszczynska-Möller, A., Fahrbach, E., Schauer, U., and Hansen, E.: Variability in Atlantic water temperature and transport at the entrance to the Arctic Ocean, 1997–2010, ICES J. Mar. Sci., 69, 852–863, 2012.

Carmack, E., Polyakov, I., Padman, L., Fer, I., Hunke, E., Hutchings, J., Jackson, J., Kelley, D., Kwok, R., Layton, C., Melling, H., Perovich, D., Persson, O., Ruddick, B., Timmermans, M.-L., Toole, J., Ross, T., Vavrus, S., and Winsor, P.: Toward quantifying the increasing role of oceanic heat in sea ice loss in the new Arctic (2015), BAMS, 96, 2079–2105, https://doi.org/10.1175/BAMS-D-13-00177.1, 2015.

Daru, V. and Tenaud, C.: High order one-step monotonicity preserving schemes for unsteady flow calculations, J. Comput. Phys., 193, 563–594, 2004.

Ferreira, D., Marshall, J., Bitz, C. M., Solomon, S., and Plumb, A.: Antarctic ocean and sea ice response to ozone depletion: a two-time-scale problem, J. Climate, 28, 1206–1226, https://doi.org/10.1175/JCLI-D-14-00313.1, 2015.

Gent, P. R. and McWilliams, J. C.: Isopychnal mixing in ocean circulation models, J. Phys. Oceanogr., 20, 150–155, 1990.

Good, P., Gregory, J. M., and Lowe, J. A.: A step-response simple climate model to reconstruct and interpret AOGCM projections, Geophys. Res. Lett., 38, L01703, https://doi.org/10.1029/2010GL045208, 2011.

Good, P., Gregory, J. M., Lowe, J. A., and Andrews, T.: Abrupt CO_2 experiments as tools for predicting and understanding CMIP5 representative concentration pathway projections, Clim. Dynam., 40, 1041–1053, https://doi.org/10.1007/s00382-012-1410-4, 2013.

Gouretski, V. V. and Koltermann, K. P.: WOCE Global Hydrographic Climatology, 35/2004, Berichte des Bundesamtes fur Seeschifffahrt und Hydrographie, 52 pp., 2004 (data available at: https://rda.ucar.edu/datasets/ds285.4/).

Gregory, J. M., Andrews, T., and Good, P.: The inconstancy of the transient climate response parameter under increasing CO_2, Philos. T. R. Soc. A, 373, 20140417, https://doi.org/10.1098/rsta.2014.0417, 2015.

Haine, T. W. N., Curry, B., Gerdes, R., Hansen, E., Karcher, M., Lee, C., Rudels, B., Spreen, G., de Steur, L., Stewart, K. D., and Woodgate, R.: Arctic freshwater export: Status, mechanisms, and prospects, Global Planet. Change, 125, 13–35, https://doi.org/10.1016/j.gloplacha.2014.11.013, 2015.

Hansen, J., Sato, M., Kharecha, P., and von Schuckmann, K.: Earth's energy imbalance and implications, Atmos. Chem. Phys., 11, 13421–13449, https://doi.org/10.5194/acp-11-13421-2011, 2011.

Hasselmann, K., Sausen, R., Maier-Reimer, E., and Voss, R.: On the cold start problem in transient simulations with coupled atmosphere-ocean models, Clim. Dynam., 9, 53–61, https://doi.org/10.1007/BF00210008, 1993.

Heimbach, P., Menemenlis, D., Losch, M., Campin, J.-M., and Hill, C.: On the formulation of sea-ice models, Part 2: Lessons from multi-year adjoint sea ice export sensitivities through the Canadian Arctic Archipelago, Ocean Model., 33, 145–158, https://doi.org/10.1016/j.ocemod.2010.02.002, 2010.

Ilicak, M., Drange, H., Wang, Q., Gerdes, R., Aksenov, Y., Bailey, D., Bentsen, M., Biastoch, A., Bozec, A., Böning, C., Cassou, C., Chassignet, E., Coward, A. C., Curry, B., Danabasoglu, G., Danilov, S., Fernandez, E., Fogli, P. G., Fujii, Y., Griffies, S. M., Iovino, D., Jahn, A., Jung, T., Large, W. G., Lee, C., Lique, C., Lu, J., Masina, S., Nurser, A. J. G., Roth, C., Salas y Mélia, D., Samuels, B. L., Spence, P., Tsujino, H., Valcke, S., Voldoire, A., Wang, X., and Yeager, S. G.: An assessment of the Arctic Ocean in a suite of interannual CORE-II simulations, Part III: Hydrography and fluxes, Ocean Model., 100, 141–161, 2016.

Jackett, D. R. and McDougall, T. J.: Minimal adjustment of hydrographic profiles to achieve static stability, JAOT, 12, 381–389, 1995.

Large, W. G. and Pond, S.: Open ocean momentum flux measurements in moderate to strong winds, J. Phys. Oceanogr, 11, 324–336, https://doi.org/10.1175/1520-0485(1981)011<0324:OOMFMI>2.0.CO;2, 1981.

Large, W. G., McWilliams, J. C., and Doney, S. C.: Oceanic vertical mixing: a review and a model with a nonlocal boundary layer parameterization, Rev. Geophys., 32, 363–403, 1994.

Lique, C., Johnson, H. L., and Davis, P. E. D.: On the interplay between the circulation in the surface and the intermediate layers on the Arctic Ocean, J. Phys. Oceanogr., 45, 1393–1409, https://doi.org/10.1175/JPO-D-14-0183.1, 2015.

Losch, M., Menemenlis, D., Campin, J.-M., Heimbach, P., and Hill, C.: On the formulation of sea-ice models, Part 1: Effects of different solver implementations and parameterizations, Ocean Model., 33, 129–144, https://doi.org/10.1016/j.ocemod.2009.12.008, 2010.

Manucharyan, G. E. and Spall, M. A.: Wind-driven freshwater buildup and release in the Beaufort Gyre constrained by mesoscale eddies, Geophys. Res. Lett., 43, 273–282, https://doi.org/10.1002/2015GL065957, 2016.

Manucharyan, G. E., Spall, M. A., and Thompson, A. F.: A theory of the wind-driven Beaufort Gyre variability, J. Phys. Oceanogr., 46, 3263–3278, 2016.

Marshall, J., Adcroft, A., Hill, C., Perelman, L., and Heisey, C.: A finite-volume, incompressible Navier–Stokes model for studies of the ocean on parallel computers, J. Geophys. Res., 102, 5753–5766, 1997a.

Marshall, J., Hill, C., Perelman, L., and Adcroft, A.: Hydrostatic, quasihydrostatic and nonhydrostatic ocean modeling, J. Geophys. Res., 102, 5733–5752, 1997b.

Marshall, J., Armour, K. C., Scott, J. R., Kostov, Y., Hausmann, U., Ferreira, D., Shepherd, T. G., and Bitz, C. M.: The ocean's role in polar climate change: asymmetric Arctic and Antarctic responses to greenhouse gas and ozone forcing, Philos. T. R. Soc. A, 372, 20130040, https://doi.org/10.1098/rsta.2013.0040, 2014.

Nguyen, A. T., Menemenlis, D., and Kwok, R.: Arctic ice-ocean simulation with optimized model parameters: approach and assessment, J. Geophys. Res., 116, C04025, https://doi.org/10.1029/2010JC006573, 2011.

Nummelin, A., Li, C., and Smedsrud, L. H.: Response of Arctic Ocean stratification to changing river runoff in a column model, J. Geophys. Res.-Oceans, 120, 2655–2675, https://doi.org/10.1002/2014JC010571, 2015.

Nummelin, A., Ilicak, M., Li, C., and Smedsrud, L. H.: Consequences of future increased Arctic runoff on Arctic Ocean stratification, circulation, and sea ice cover, J. Geophys. Res.-Oceans, 121, 617–637, https://doi.org/10.1002/2015JC011156, 2016.

Pemberton, P. and Nilsson, J.: The response of the central Arctic Ocean stratification to freshwater perturbations, J. Geophys. Res.-Oceans, 121, 792–817, https://doi.org/10.1002/2015JC011003, 2016.

Proshutinsky, A. and Johnson, M.: Two circulation regimes of the wind-driven Arctic Ocean, J. Geophys. Res., 102, 12493–12514, 1997.

Proshutinsky, A., Bourke, R. H., and McLaughlin, F. A.: The role of the Beaufort Gyre in Arctic climate variability: seasonal to decadal climate scales, Geophys. Res. Lett., 29, 2100, https://doi.org/10.1029/2002GL015847, 2002.

Proshutinsky, A., Krishfield, R., Timmermans, M.-L., Toole, J., Carmack, E., McLaughlin, F., Williams, W. J., Zimmermann, S., Itoh, M., and Shimada, K.: Beaufort Gyre freshwater reservoir: State and variability from observations, J. Geophys. Res., 114, C00A10, https://doi.org/10.1029/2008JC005104, 2009.

Proshutinsky, A., Aksenov, Y., Clement Kinney, J., Gerdes, R., Golubeva, E., Holland, D., Holloway, G., Jahn, A., Johnson, M., Popova, E., Steele, M., and Watanabe, E.: Recent advances in Arctic ocean studies employing models from the Arctic Ocean Model Intercomparison Project, Oceanography, 24, 102–113, https://doi.org/10.5670/oceanog.2011.61, 2011.

Proshutinsky, A., Dukhovskoy, D., Timmermans,M- L., Krishfield, R., and Bamber, J.: Arctic circulation regimes, Philos. T. R. Soc. A, 373, 20140160, https://doi.org/10.1098/rsta.2014.0160, 2015.

Rabe, B., Karcher, M., Kauker, F., Schauer, U., Toole, J. M., Krishfield, R. A., Pisarev, S., Kikuchi, T., and Su, J.: Arctic Ocean basin liquid freshwater storage trend 1992–2012, Geophys. Res. Lett., 41, 961–968, https://doi.org/10.1002/2013GL058121, 2014.

Rigor, I. G., Wallace, J. M., and Colony, R. L.: Response of sea ice to the arctic oscillation, J. Climate, 15, 2648–2663, 2002.

Smith, W. H. F. and Sandwell, D. T.: Global seafloor topography from satellite altimetry and ship depth soundings, Science, 277, 1956–1962, 1997.

Thompson, D. W. J. and Wallace, J. M.: The Arctic Oscillation signature in the wintertime geopotential height and temperature fields, Geophys. Res. Lett., 25, 1297–1300, 1998.

Thompson, D. W. J. and Wallace, J. M.: Regional climate impacts of the northern hemisphere annular mode, Science, 293, 85–89, 2001.

Toole, J. M., Timmermans, M.-L., Perovich, D. K., Krishfield, R. A., Proshutinsky, A., and Richter-Menge, J. A.: Influences of the ocean surface mixed layer and thermohaline stratification on Arctic Sea Ice in the Central Canada basin, J. Geophys. Res., 115, C10018, https://doi.org/10.1029/2009JC005660, 2010.

Woodgate, R. A., Stafford, K. M., and Prahl, F. G.: A synthesis of year-round interdisciplinary mooring measurements in the Bering Strait (1990–2014) and the RUSALCA years (2004–2011), Oceanography, 28, 46–67, https://doi.org/10.5670/oceanog.2015.57, 2015.

Yang, Q., Dixon, T. H., Myers, P. G., Bonin, J., Chambers, D., van den Broeke, M. R., Ribergaard, M. H., and Mortensen, J.: Recent increases in Arctic freshwater flux affects Labrador Sea convection and Atlantic overturning circulation, Nat. Commun., 7, 10525, https://doi.org/10.1038/ncomms10525, 2016.

Joint Program Reprint Series - Recent Articles

For limited quantities, Joint Program publications are available free of charge. Contact the Joint Program office to order.
Complete list: http://globalchange.mit.edu/publications

2017-22 "Climate response functions" for the Arctic Ocean: a proposed coordinated modelling experiment. Marshall, J., J. Scott and A. Proshutinsky, *Geoscientific Model Development* 10: 2833–2848 (2017)

2017-21 Aggregation of gridded emulated rainfed crop yield projections at the national or regional level. Blanc, É., *Journal of Global Economic Analysis* 2(2): 112–127 (2017)

2017-20 Historical greenhouse gas concentrations for climate modelling (CMIP6). Meinshausen, M., E. Vogel, A. Nauels, K. Lorbacher, N. Meinshausen, D. Etheridge, P. Fraser, S.A. Montzka, P. Rayner, C. Trudinger, P. Krummel, U. Beyerle, J.G. Cannadell, J.S. Daniel, I. Enting, R.M. Law, S. O'Doherty, R.G. Prinn, S. Reimann, M. Rubino, G.J.M. Velders, M.K. Vollmer, and R. Weiss, *Geoscientific Model Development* 10: 2057–2116 (2017)

2017-19 The Future of Coal in China. Zhang, X., N. Winchester and X. Zhang, *Energy Policy,* 110: 644–652 (2017)

2017-18 Developing a Consistent Database for Regional Geologic CO2 Storage Capacity Worldwide. Kearns, J., G. Teletzke, J. Palmer, H. Thomann, H. Kheshgi, H. Chen, S. Paltsev and H. Herzog, *Energy Procedia*, 114: 4697–4709 (2017)

2017-17 An aerosol activation metamodel of v1.2.0 of the pyrcel cloud parcel model: development and offline assessment for use in an aerosol–climate model. Rothenberg, D. and C. Wang, *Geoscientific Model Development,* 10: 1817–1833 (2017)

2017-16 Role of atmospheric oxidation in recent methane growth. Rigby, M., S.A. Montzka, R.G. Prinn, J.W.C. White, D. Young, S. O'Doherty, M. Lunt, A.L. Ganesan, A. Manning, P. Simmonds, P.K. Salameh, C.M. Harth, J. Mühle, R.F. Weiss, P.J. Fraser, L.P. Steele, P.B. Krummel, A. McCulloch and S. Park, *Proceedings of the National Academy of Sciences,* 114(21): 5373–5377 (2017)

2017-15 A revival of Indian summer monsoon rainfall since 2002. Jin, Q. and C. Wang, *Nature Climate Change,* 7: 587–594 (2017)

2017-14 A Review of and Perspectives on Global Change Modeling for Northern Eurasia. Monier, E., D. Kicklighter, A. Sokolov, Q. Zhuang, I. Sokolik, R. Lawford, M. Kappas, S. Paltsev and P. Groisman, *Environmental Research Letters*, 12(8): 083001 (2017)

2017-13 Is Current Irrigation Sustainable in the United States? An Integrated Assessment of Climate Change Impact on Water Resources and Irrigated Crop Yields. Blanc, É., J. Caron, C. Fant and E. Monier, *Earth's Future*, 5(8): 877–892 (2017)

2017-12 Assessing climate change impacts, benefits of mitigation, and uncertainties on major global forest regions under multiple socioeconomic and emissions scenarios. Kim, J.B., E. Monier, B. Sohngen, G.S. Pitts, R. Drapek, J. McFarland, S. Ohrel and J. Cole, *Environmental Research Letters*, 12(4): 045001 (2017)

2017-11 Climate model uncertainty in impact assessments for agriculture: A multi-ensemble case study on maize in sub-Saharan Africa. Dale, A., C. Fant, K. Strzepek, M. Lickley and S. Solomon, *Earth's Future* 5(3): 337–353 (2017)

2017-10 The Calibration and Performance of a Non-homothetic CDE Demand System for CGE Models. Chen, Y.-H.H., *Journal of Global Economic Analysis* 2(1): 166–214 (2017)

2017-9 Impact of Canopy Representations on Regional Modeling of Evapotranspiration using the WRF-ACASA Coupled Model. Xu, L., R.D. Pyles, K.T. Paw U, R.L. Snyder, E. Monier, M. Falk and S.H. Chen, *Agricultural and Forest Meteorology*, 247: 79–92 (2017)

2017-8 The economic viability of Gas-to-Liquids technology and the crude oil-natural gas price relationship. Ramberg, D.J., Y.-H.H. Chen, S. Paltsev and J.E. Parsons, *Energy Economics*, 63: 13–21 (2017)

2017-7 The Impact of Oil Prices on Bioenergy, Emissions and Land Use. Winchester, N. and K. Ledvina, *Energy Economics*, 65(2017): 219–227 (2017)

2017-6 The impact of coordinated policies on air pollution emissions from road transportation in China. Kishimoto, P.N., V.J. Karplus, M. Zhong, E. Saikawa, X. Zhang and X. Zhang, *Transportation Research Part D*, 54(2017): 30–49 (2017)

2017-5 Twenty-First-Century Changes in U.S. Regional Heavy Precipitation Frequency Based on Resolved Atmospheric Patterns. Gao, X., C.A. Schlosser, P.A. O'Gorman, E. Monier and D. Entekhabi, *Journal of Climate*, online first, doi: 10.1175/JCLI-D-16-0544.1 (2017)

2017-4 The CO_2 Content of Consumption Across U.S. Regions: A Multi-Regional Input-Output (MRIO) Approach. Caron, J., G.E. Metcalf and J. Reilly, *The Energy Journal*, 38(1): 1–22 (2017)

2017-3 Human Health and Economic Impacts of Ozone Reductions by Income Group. Saari, R.K., T.M. Thompson and N.E. Selin, *Environmental Science & Technology*, 51(4): 1953–1961 (2017)

2017-2 Biomass burning aerosols and the low-visibility events in Southeast Asia. Lee, H.-H., R.Z. Bar-Or and C. Wang, *Atmospheric Chemistry & Physics*, 17, 965–980 (2017)

2017-1 Statistical emulators of maize, rice, soybean and wheat yields from global gridded crop models. Blanc, É., *Agricultural and Forest Meteorology,* 236, 145–161 (2017)

2016-25 Reducing CO_2 from cars in the European Union. Paltsev, S., Y.-H.H. Chen, V. Karplus, P. Kishimoto, J. Reilly, A. Löschel, K. von Graevenitz and S. Koesler, *Transportation*, online first (doi:10.1007/s11116-016-9741-3) (2016)

MIT Joint Program on the Science and Policy of Global Change

Massachusetts Institute of Technology
77 Massachusetts Ave., E19-411
Cambridge MA 02139-4307 (USA)

T (617) 253-7492 F (617) 253-9845
globalchange@mit.edu
http://globalchange.mit.edu